Optimal LGS pointing with a faint tip-tilt NGS

Richard Dekany

Caltech Optical Observatories, MS 11-17, Pasadena, CA 91125, USA

ABSTRACT

Experience with the current generation of astronomical single laser guide star (LGS) adaptive optics (AO) systems has demonstrated system performance that is often limited by residual tip-tilt errors induced by the paucity of bright tip-tilt natural guide stars (NGS). To overcome this limitation, we are developing a new generation of tip-tilt sensors that will operate at near-infrared wavelengths where the NGS is sharpened to the diffraction limit. To optimize performance, single LGS AO systems utilizing sharpened tip-tilt NGS should generally not point their LGS directly toward their science target. Rather, optimal performance for wide sky coverage is obtained by offsetting LGS pointing along a radius connecting the science target and the tip-tilt NGS. We demonstrate that determination of the jointly optimized LGS pointing angle and tip-tilt wavefront sensor (WFS) integration time can improve performance metrics by factors of several, particularly for faintest NGS operation. We find the LGS offset should be as much as 1/2 the distance to the NGS to maximize Strehl ratio at near-infrared wavelengths and $\approx 1/4$ the distance to the NGS to maximize ensquared energy, with lesser off-pointing for brighter NGS. Future AO systems may benefit from predictive determination of optimal LGS offsetting, based upon changing atmospheric conditions and observational geometries.

Keywords: Tip-tilt sensing, adaptive optics, laser guide star, wavefront sensing

1. INTRODUCTION

Future laser guide star (LGS) adaptive optics (AO) systems developed for astronomical telescopes will increasingly bifurcate into two classes: wide-field-of-view, partial-compensation AO systems and narrow field-of-view, precision AO systems. The former is rather tolerant of residual tip-tilt errors due to the relatively large diameter point spread function (PSF) inherent in such systems. The latter, providing a PSF width approaching the limit set by photon diffraction, will demand the very best tip-tilt error compensation available, which currently requires optimal exploitation of available NGS.

Precision LGS AO science on telescopes of all sizes can benefit from improved tip-tilt error rejection.[1] On small aperture telescopes, significant residual atmospheric tip-tilt measurement and bandwidth error and tilt anisoplanatism lead to large tip-tilt residuals. On the largest aperture telescopes,[2] the benefits of large collecting area and finite outer scale significantly decrease tip-tilt wavefront error energy, but these large structures are increasingly susceptible to new sources of error accentuated by exquisitely narrow PSF such as pointing jitter induced by the telescope drives, direct wind buffeting of the telescope structure, correlated segment wind shake,[3] and transfer of wind buffeting on the dome to the telescope pier through surrounding soil.[4]

Currently, LGS AO systems utilize visible-light NGS signal to determine tip-tilt errors in the science wavefront, typically because this optimizes light collecting efficiency for near-infrared science and because low noise CCD or noiseless APD visible detector systems have been readily available. Unfortunately, the tip-tilt measuring performance using only partially-corrected visible PSF's results in rather large tip-tilt errors when guiding on the faintest NGS. To improve tip-tilt performance, we are developing a new generation of tip-tilt wavefront sensors that will enjoy improved measurement accuracy by operating at near-infrared wavelengths with low detector noise, where AO correction to the diffraction-limited PSF width is routinely achieved. In return, we are driven to more complicated observing scenarios, typically involving the utilization of one or more near-infrared observing bands for tip-tilt wavefront sensing, while a different observing band is used simultaneously for science observations.

Further author information: (Send correspondence to R.G.D.)
R.G.D.: E-mail: rgd@astro.caltech.edu, Telephone: 1 626 395 6798

Adaptive Optics Systems II, edited by Brent L. Ellerbroek, Michael Hart, Norbert Hubin, Peter L. Wizinowich,
Proc. of SPIE Vol. 7736, 773625 · © 2010 SPIE · CCC code: 0277-786X/10/$18 · doi: 10.1117/12.857841

2. SCIENCE TARGET STREHL RATIO

The science target Strehl ratio, S_{Sci}, is given by the product of the high-order wavefront error Strehl, S_{HO}, and the tip-tilt error Strehl, S_T,

$$S_{Sci} = S_{HO} * S_T \tag{1}$$

It is worth noting that the two terms contributing to science target Strehl ratio have different angular dependencies, described below, which is the fundamental driver that determines the optimal LGS pointing direction.

2.1 High-order Wavefront Error Strehl Ratio

For precision wavefront correction, the high-order wavefront error Strehl can be reasonably approximated via the Marechal approximation,[5]

$$S_{HO} = e^{-\sigma_{HO}^2} \tag{2}$$

where σ_{HO} is the tip-tilt removed root-mean-square (RMS) residual wavefront error composed of various error source terms, that can broadly be considered to contribute independently to an overall error variance,

$$\sigma_{HO}^2 = \sigma_{AA}^2 + \sigma_B^2 + \sigma_F^2 + \sigma_{FA}^2 + \sigma_M^2 + \sigma_{Other}^2 \tag{3}$$

where σ_M, measurement error and σ_B, system temporal bandwidth error, arise from the need to collect wavefront information from the guide star of appropriate signal-to-noise ration (SNR) and the finite time required to process wavefront sensor information into deformable mirror (DM) commands. All AO systems will also suffer from σ_F, fitting error, due to finite correction spatial bandwidth. Single LGS AO systems will suffer σ_{FA}, focal anisoplanatism error (while multiple LGS AO systems suffer instead from residual tomography error not considered here.) Single conjugate AO systems suffer from σ_{AA}, angular anisoplanatism between LGS pointing direction and science target, while multi-conjugate adaptive optics will suffer instead from generalized anisoplanatism across the science field of view, again not considered in the scope of this study. Finally, σ_{Other} includes errors due to wavefront sensor aliasing, scintillation, chromatic errors, and any number of engineering implementation errors, such as DM hysteresis, WFS non-linearity, and wavefront calibration errors. In reality, the assumption of error independence somewhat overestimates the potential on-sky performance, but this second-order effect does not affect our basic conclusions here.

2.1.1 Angular anisoplanatism error

The high-order wavefront error due to angular anisoplanatism when a wavefront is measured from a direction differing by angle θ from the direction of the science target is given by

$$\sigma_{AA} = \left(\frac{\theta}{\theta_0}\right)^{5/6} \text{[rad of phase]} \tag{4}$$

where θ_0 is the isoplanatic angle which is a function of the $\frac{5}{3}$ vertical turbulence moment of the $C_n^2(h,t)$ profile.[6]

2.1.2 Bandwidth and delay errors

The residual high-order wavefront error due to finite temporal bandwidth and pure-delay errors is given by

$$\sigma_B = \sqrt{\kappa \left(\frac{f_G}{f_S}\right)^{5/3} + 28.4\,(T_{Delay} f_G)^{5/3}} \text{ [rad of phase]} \tag{5}$$

where f_G is the Greenwood frequency, f_S is the AO system correction servo bandwidth, and κ is a coefficient that depends on the implementation of the servo control law ($\kappa = 1$ for a single-pole control law).[7] For a single turbulent layer, where $f_G = 0.427\,v/r_0$, this can be simplified to be

$$\sigma_B = \sqrt{\left(\frac{0.427v}{r_0 f_S}\right)^{5/3} + \left(\frac{0.427 v T_{Delay}}{r_0}\right)^{5/3}} = \sqrt{35.7\left(\frac{vT_{Int}}{r_0}\right)^{5/3} + 6.88\left(\frac{vT_{Delay}}{r_0}\right)^{5/3}} \text{ [rad of phase]} \tag{6}$$

for an AO system whose servo bandwidth is inversely related to WFS integration time, T_{Int}, via $f_S = 0.05/T_{Int}$, a relationship typical of a well-designed controller.

The effective time delay for any closed-loop AO system is at least the integration time (1/2 the WFS integration time plus 1/2 the DM hold time). For now, we will assume $T_{Delay} = 2\,T_{Int}$ and can thus summarize

$$\sigma_B = 7.58\left(\frac{vT_{Int}}{r_0}\right)^{5/6} \text{ [rad of phase]} \tag{7}$$

2.1.3 Fitting error

The high-order wavefront error due to finite spatial bandwidth of a wavefront corrector can be described as

$$\sigma_F = \alpha\left(\frac{D}{\Delta x}\right)^{5/6} \text{ [rad of phase]} \tag{8}$$

where α is a coefficient that depends on the corrector type and influence function, and Δx is the corrector spacing, as projected onto the telescope primary mirror. For our purpose here, we wish to consider thin facesheet deformable mirrors[7] having $\alpha \approx 0.28$.

2.1.4 Focal anisoplanatism error

The high-order wavefront error due to focal anisoplanatism in a single LGS system is given by

$$\sigma_{FA} = \left(\frac{D}{d_0}\right)^{5/6} \text{ [rad of phase]} \tag{9}$$

where d_0 is the focal anisoplanatism coherence diameter which is a function of μ_2, the second vertical moment of the $C_n^2(h,t)$ profile.

2.1.5 Measurement error

The residual high-order wavefront error due to imperfect measurement can be described for a Shack-Hartmann wavefront sensor (WFS) as[7]

$$\sigma_M = \frac{3\pi d\epsilon}{16} \frac{w_{Spot}}{\left(\frac{S}{N}\right)_{LGS}} \text{ [rad of phase]} \tag{10}$$

where w_{Spot} is the full-width at half-maximum (FWHM) of the guide star short exposure electronic PSF at the LGS WFS focal plane [radians of angle on sky], $(\frac{S}{N})_{LGS}$ in the signal-to-noise ratio of the subaperture detection, d is the subaperture diameter $d = D/N_{Subap}$ [meters], and ϵ is the error propagator for reconstruction, for which we will assume a Fried geometry.[7] Our model for subaperture image width is given by,

$$w_{Spot} \approx \sqrt{\left(\frac{\lambda_{LGS} N_{Subap}}{D}\right)^2 + \left(\frac{\lambda_{LGS}}{r_0}\right)^2 + \sigma^2_{ChargeDiffusion}} \tag{11}$$

$$\epsilon \approx \sqrt{0.190 + 0.107 \ln N^2_{Subap}} \tag{12}$$

$$\left(\frac{S}{N}\right)_{LGS} = \frac{F_{LGS}\, q_{LGS}}{\sqrt{F_{LGS} q_{LGS} + N^2_{Pix}(\sigma^2_{Read_{LGS}} + \sigma_{Dark_{LGS}} T_{Int})}} \tag{13}$$

$$= \frac{P_{Laser} \tau_{Proj} \eta_c D^2 T_{Int} \tau^2_{Atm}\, q_{LGS}}{\sqrt{P_{Laser} \tau_{Proj} \eta_c D^2 N^2_{Subap} T_{Int} \tau^2_{Atm} q_{LGS} + N^4_{Subap} N^2_{Pix} (T_{Int} \sigma_{Dark_{LGS}} + \sigma^2_{Read_{LGS}})}} \tag{14}$$

where λ_{LGS} is the guide star laser wavelength, N_{Subap} is the number of wavefront sensor subapertures across the telescope pupil diameter, r_0 is the atmospheric coherence parameter (at λ_{LGS}), $\sigma_{ChargeDiffusion}$ is the electronic broadening of the PSF after photodetection, q_{LGS} is the quantum efficiency of the LGS WFS detector, N_{Pix} is the number of pixels across the diameter of a LGS WFS subaperture, F_{LGS} is the laser return at the entrance pupil of the telescope [$ph\ m^{-2}\ s^{-1}$], η_c is the laser return coupling efficiency to the sodium layer, $\sigma_{Read_{LGS}}$ is the root-mean-squared (RMS) readout noise of the LGS WFS [$e-$], $\sigma_{Dark_{LGS}}$ is the dark current variance in the LGS WFS [$e-\ s^{-1}$], P_{Laser} is the guide star laser power [W] at the output of the laser itself, τ_{Atm} is the atmospheric transmission at LGS wavelength, τ_{Proj} is the LGS beam transport and projector system transmission at LGS wavelength, T_{Int} is the WFS integration time.

2.1.6 Other high-order wavefront errors

Any practical AO system will also suffer from a number of smaller atmospheric and implementation errors, such as WFS aliasing error, chromatic errors that arise when observing off-zenith, internal calibration errors, and non-common-path errors between AO system and science instrument.

$$\sigma_{Other} = \text{Constant [rad of phase]} \tag{15}$$

2.2 Science Target Tip-tilt Error Strehl Ratio

The science target Strehl ratio due to tip-tilt errors from (1) can be written[8]

$$S_T = \frac{1}{1 + \frac{\pi^2}{2}\left(\frac{\sigma_T}{\lambda_{Sci}/D}\right)^2} \tag{16}$$

where σ_T is the 1-axis RMS residual tilt error in the science wavefront, λ_{Sci} is the science observing wavelength, and D is the telescope entrance pupil diameter. We can expand by assuming independence of error terms to write

$$\sigma_T = \sqrt{\sigma_{TM}^2 + \sigma_{TB}^2 + \sigma_{TAA}^2 + \sigma_{TOther}^2} \tag{17}$$

where σ_{TM} is the measurement error from the NGS-based tip-tilt measurement defined in analogy to (10) above, σ_{TB} is the tip-tilt bandwidth error, and σ_{TAA} is 1-axis tilt anisoplanatism, which corresponds to angular anisoplanatism for the tip-tilt wavefront modes.

2.2.1 Tilt bandwidth error

Residual science path tip-tilt error depends upon the latency of the tip-tilt measurement, as well as L_0, the outer scale of atmospheric turbulence. Under the frozen flow assumption,

$$\sigma_{TB} = 0.177 \left(\frac{T_{TInt}}{\tau_0}\right) \left(\frac{\lambda_{Tilt}}{D}\right) \left(\frac{r_0}{D}\right)^{\frac{1}{6}} \text{[rad of phase]} \tag{18}$$

where T_{TInt} is the integration time in the tip-tilt sensor, λ_{Tilt} is the tip-tilt sensing wavelength, τ_0 is the atmospheric coherence time which depends upon atmospheric turbulence strength and wind speed, including the effect of L_0, the outer scale of turbulence.[7]

2.2.2 Tilt anisoplanatism error

Tilt anisoplanatism arises when wavefront tilt measurements are made in a direction differing by angle θ from the direction of the science target, and can be described for small angles by[6]

$$\sigma_{TAA} = 2.31 \sqrt{1 - 20.6 \left(\frac{D}{L_0}\right)^2 + 27.4 \left(\frac{D}{L_0}\right)^{7/3}} \sqrt{\frac{\theta^2 \mu_2}{D^{7/3}}} \text{[rad of phase]} \tag{19}$$

where μ_2 is the second moment of the turbulence distribution[7] and we have assumed the 1-axis average of the radial and tangential tilt anisoplanatism terms.

2.3 Science Target Ensquared Energy

The concentration of science light into either an imager or spectrograph detection element is appropriately described, for narrow spectral bandwidth, by the ensquared energy (EE), which is related to the AO system point spread function (PSF) by

$$\text{EE} = \int_{-s/2}^{s/2} \int_{-s/2}^{s/2} PSF(x, y)\, dx dy \tag{20}$$

To investigate the noise properties of fast guiding on sharpened tip-tilt stars, we can approximate the PSF in the regime of good AO correction as the convolution of a diffraction-limited image core (approximated by a Gaussian function), containing a fraction of energy corresponding to the Strehl ratio, and a blurring kernel that is also described by a Gaussian of width related to the two-dimensional residual tip-tilt error

$$PSF(x, y) \propto S_{HO} \exp\left(-\frac{x^2 + y^2}{2\left(0.437\lambda/D\right)^2}\right) \otimes \exp\left(-\frac{x^2 + y^2}{2\sigma_{1-D}^2}\right) \tag{21}$$

Using (21), we can determine the EE analytically based upon the residual tip-tilt error in the science target wavefront, as determined in (17).

3. AO SYSTEM AND ATMOSPHERE MODELS

We are motivated for this study to consider the potential performance of optimal LGS pointing when used in combination with a near-infrared wavelength tip-tilt sensor to be developed for the workhorse Keck 2 LGS AO system[3] at the W. M. Keck Observatory on Mauna Kea. Our system will allow reconfiguration so that J and H-band science observations can be performed, while using K-band for tip-tilt sensing anywhere in the AO system field of regard, or alternatively K-band science can be performed within a central 35 arcsecond diameter field, with tip-tilt sensing in K-band utilizing NGS outside this central field. As the AO system high-order correction is improved over time, the potential also exists to utilize H or J-bands for tip-tilt sensing.

To make concrete selections for our study, we adopt the parameters shown in Table 1 as specific to the Keck 2 AO system (as envisioned in the near future), where τ represents optical transmission, q quantum efficiency, and σ_{Read} and σ_{Dark} the detector read noise and dark current noise as used in (14). The subscripts LGS refer to the high-order laser guide star wavefront sensor, while subscripts NGS correspond to the near-infrared NGS tip-tilt wavefront sensor.

Table 1. Basic AO system model parameter used in this paper. Deviations from these parameters are noted in the text when appropriate.

Telescope Model Parameter	**Value**
D	10 m
N_{Subap}	20
N_{Pix}	4
τ_{Proj}	0.60
τ_{Atm}	0.892
$\tau_{AO_{LGS}}$	0.85
q_{LGS}	0.85
$\sigma_{ChargeDiffusion}$	0.5 pixel FWHM
τ_{TTS}	0.85
q_{TTS}	0.80
λ_{LGS}	589 nm
$\sigma_{ReadLGS}$	2.2 e- RMS
$\sigma_{DarkLGS}$	265 e-/sec/pixel
$\sigma_{ReadTTS}$	3.5 e- RMS
$\sigma_{DarkTTS}$	1 e-/sec/pixel
P_{Laser}	20 W CW
Mesospheric Na Return	75 photons $cm^{-2}s^{-1}W^{-1}$
σ_{Other}	90 nm RMS
$\sigma_{TTOther}$	1.0 mas RMS
IFS spaxel size (H-band)	62 mas

4. STREHL PERFORMANCE WITH LGS POINTING

Having developed the expanded forms for (3) above, we can now proceed to study the behavior of LGS AO system performance in regimes limited by either residual high-order wavefront errors or by residual tip-tilt error terms. A convenient way to explore the continuum of performance regimes is to consider the AO system science

Table 2. Basic AO system model parameter used in this paper. Deviations from these parameters are noted in the text when appropriate.

Atm Model Parameter	Value
r_0	16 cm
θ_0	2.7 arcsec
d_0	4.28 m
μ_2	9.41 x 10^{-6}
L_0	30 m
Turbulence spectrum	von Karman
$v_{\text{Turbulence-weighted}}$	9.5 m s^{-1}
Zenith angle	0 deg

target performance as a function of the tip-tilt NGS brightness and off-axis distance, θ. In the following, we will consider tip-tilt NGS located at $\theta < 45$" off-axis having near-infrared brightnesses $10 < m_H (\text{or } m_K) < 17$.

Based on the performance model described above, and the AO system and atmospheric parameters described in Tables 1 and 2, we calculate the contributions to science target Strehl ratio as a function of the LGS pointing offset, θ_{LGS}, which is measured from the science target. In Figure 1, we present the behavior of S_{HO}, S_T, S_{Sci}, and S_{NGS}, the Strehl ratio of the tip-tilt NGS PSF. We see that the peak combined S_{Sci} is obtained when the LGS is offset only slightly for a tip-tilt NGS 15" off-axis (due to the relatively benign effects of angular anisoplanatism on tip-tilt NGS Strehl and tilt anisoplanatism on science target Strehl.) When the tip-tilt NGS, however, is 30" off-axis, a larger LGS pointing offset is needed to obtain best science Strehl ratio, as this provides somewhat lower σ_{TM} due to greater K-band S_{NGS} (though it is still just a few percent in the $\theta = 30$" case examined).

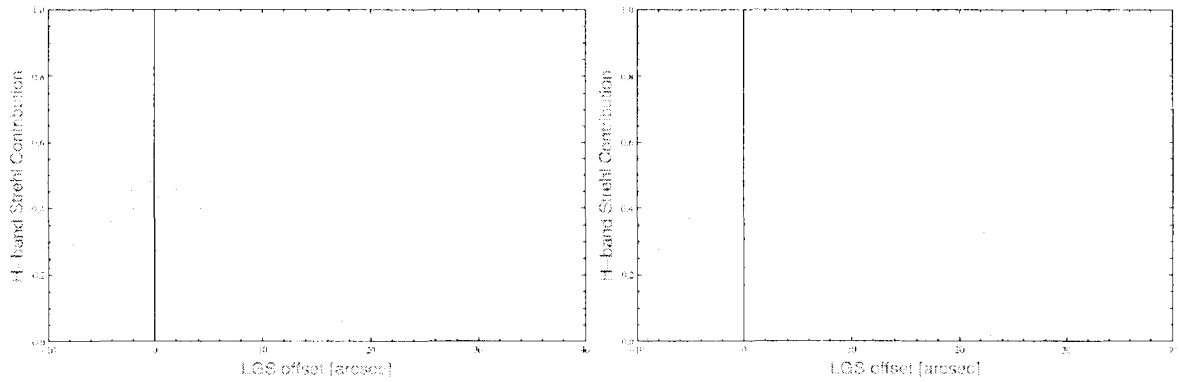

Figure 1. Science target H-band Strehl contributions for a single LGS AO observation with $m_K = 15$ tip-tilt NGS star located 15" (**left**) and 30" (**right**) from the science target. Within each figure, the tradeoff between high-order (**solid**) and tip-tilt (**large dashed**) Strehl ratio, total science Strehl ratio (**dotted**), and tip-tilt NGS Strehl ratio (**dashed**) is shown as θ_{LGS} is increased toward the tip-tilt NGS. In this model, only K-band photons are used in the tip-tilt NGS wavefront sensor, and the tip-tilt WFS integration time was held constant at 1 millisecond.

4.1 Optimizing LGS Off-pointing and Tip-tilt WFS Integration Time

To evaluate the potential gain of LGS off-pointing in a more realistic situation, we must consider the flexibility of the AO system operator to vary the tip-tilt NGS WFS integration time, T_{TInt}, to balance the SNR in the tip-tilt measurement term and the angular anisoplanatism error in the science target wavefront.

Not surprisingly, the performance contours shown indicate that for any particular LGS pointing, there is an optimal choice of T_{TInt}, with this optimal value moving to longer exposure times for decreasingly bright tip-tilt NGS. At the same time, the optimal value for $\theta_{LGS} = \theta_{LGS}^{Opt}$ moves to increasing angles for decreasing tip-tilt NGS brightness. This is because, as the tip-tilt measurement error grows with falling brightness, it is increasingly important to maintain the Strehl ratio of the tip-tilt NGS.

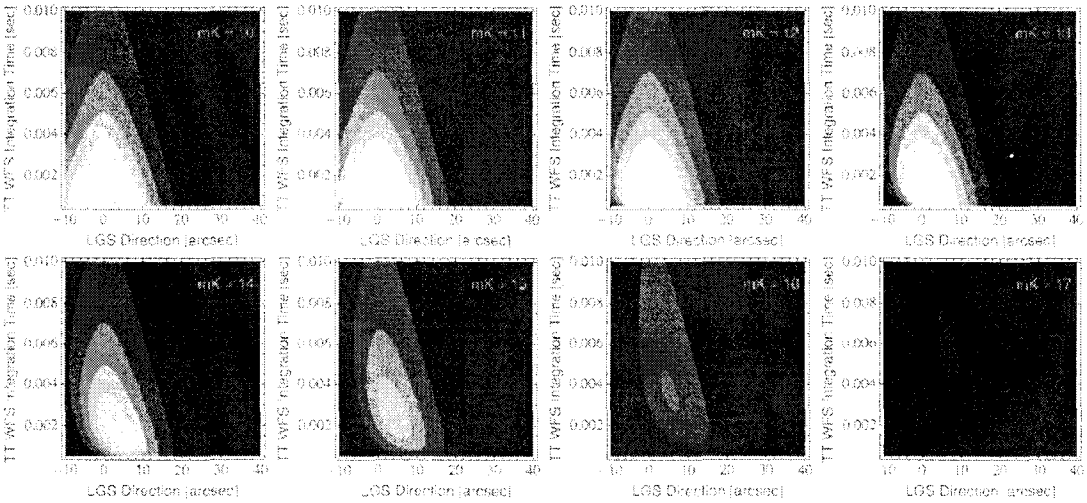

Figure 2. Science target H-band Strehl ratio performance contours for tip-tilt NGS located 30" from the science target, having magnitudes between $10 < m_K < 17$. Each frame plots Strehl ratio in 2.5% contours for a range of tip-tilt sensor integration times, T_{TInt}, and LGS pointing, θ_{LGS}.

In the case of K-band science and H-band tip-tilt wavefront sensing, the overall Strehl ratio is of course higher (Figure 3), but the trend indicates the same advantage from LGS off-pointing as the brightness of the tip-tilt NGS star decreases. At the faint limit, where science target K-band Strehl ratio is dominated by the need for the best sharpening of the tip-tilt NGS, the optimal value of θ_{LGS} is seen to be as much as 20 arcseconds in this case, or 2/3 of the distance between the science target and the off-axis tip-tilt NGS.

4.2 Potential Advantage of LGS Off-pointing

Through optimization of both θ_{LGS} and T_{TInt}, we can determine the peak performance for Strehl ratio as a function of the tip-tilt NGS off-axis distance, θ. For faint near-infrared tip-tilt NGS ($m_H = m_K = 17$), the performance comparison is shown in Figure 4. The greatest potential gain for LGS off-pointing for the scenario investigated here is seen to occur for K-band science (H-band tip-tilt sensing), when the tip-tilt NGS is off-axis by more than $\theta = 15$ arcseconds. At $\theta = 20$ arcseconds, the increase in K-band Strehl ratio is dramatic, rising from $\approx 5\%$ to nearly 20%, with a corresponding determined value of $\theta_{LGS}^{Opt} \approx 10$ arcseconds.

5. ENSQUARED ENERGY PERFORMANCE WITH LGS POINTING

Ensquared energy (EE), the fraction of light energy collected within a certain focal plane area, is more robust to residual tip-tilt errors than is Strehl ratio. Again assuming K-band light is dedicated to tip-tilt wavefront sensing, we can compare EE performance for H-band science, as shown in Figure 5 below, with that for Strehl ratio shown in Figure 2, following the PSF assumptions of (20) and (21). As one expects, EE is less sensitive to the exact choice of tip-tilt WFS integration time, T_{TInt}, resulting to performance contours elongated in the integration time dimension. Interestingly, θ_{LGS}^{Opt} is reduced, by approximately 1/2, compared to that determined to optimize Strehl ratio in Section 4.1. Still, LGS off-pointing remains an important degree of freedom to optimizing science target EE, improving EE over an on-axis projection by 30% or more in the case of the faintest guide stars.

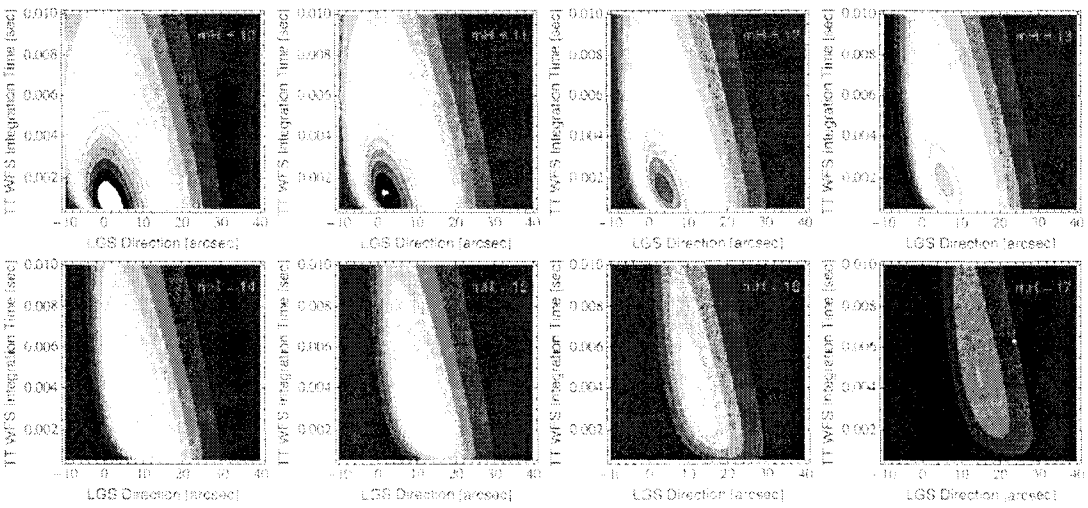

Figure 3. Science target K-band Strehl ratio performance contours for tip-tilt NGS located 30" from the science target, having magnitudes between $10 < m_K < 17$. Each frame plots Strehl ratio in 2.5% contours for a range of tip-tilt sensor integration times, T_{TInt}, and LGS pointing, θ_{LGS}.

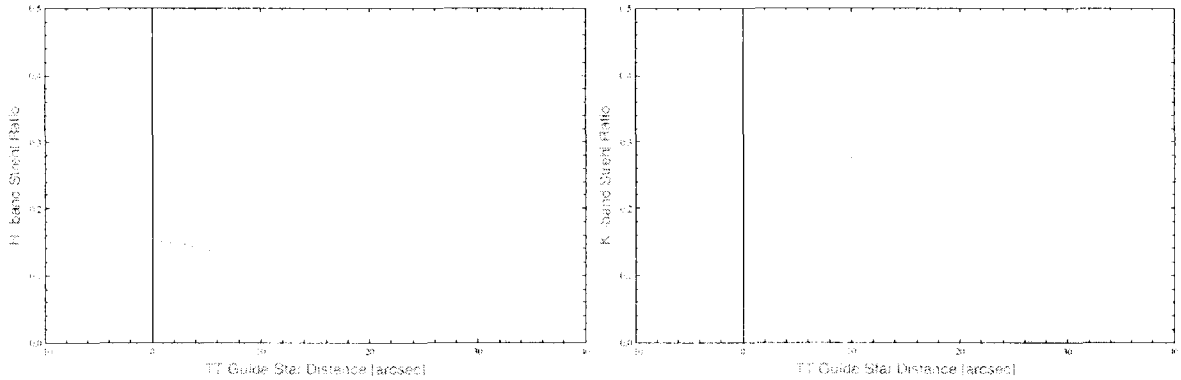

Figure 4. Science target Strehl ratio comparison for H-band (left) and K-band (right) science observations (in each case performing tip-tilt wavefront sensing with the alternate observing band). Each figure displays the Strehl ratio obtained through optimization of T_{TInt} alone for on-axis LGS pointing (**solid**) and through the joint optimization of T_{TInt} and θ_{LGS} (**dashed**).

6. CONCLUSIONS

Adaptive optics sharpening of tip-tilt NGS will provide significant increases in AO system performance metrics, such as Strehl ratio and ensquared energy. When exploiting the SNR advantage of diffraction-limited tip-tilt NGS, however, future AO systems will have available (and indeed will be required to exploit) a new degree of operating freedom, namely the direction for LGS projection. As θ_{LGS}, the distance between LGS and science target is increased, angular anisoplanatism error will begin to reduce the science target Strehl attributable to high-order wavefront errors. This effect, however, can be more than compensated by the improvement in the tip-tilt error contribution to Strehl ratio brought about through better tip-tilt NGS sharpening, particularly in the case of faint NGS. We find θ_{LGS}^{Opt} can be as large as $\theta/2$, half the angular distance to the tip-tilt NGS, in the case of optimizing near-infrared band Strehl ratio with particularly faint NGS. For optimizing ensquared energy, we find it more common to find $\theta_{LGS}^{Opt} = \theta/4$, with smaller offsets in both cases when using brighter tip-tilt NGS.

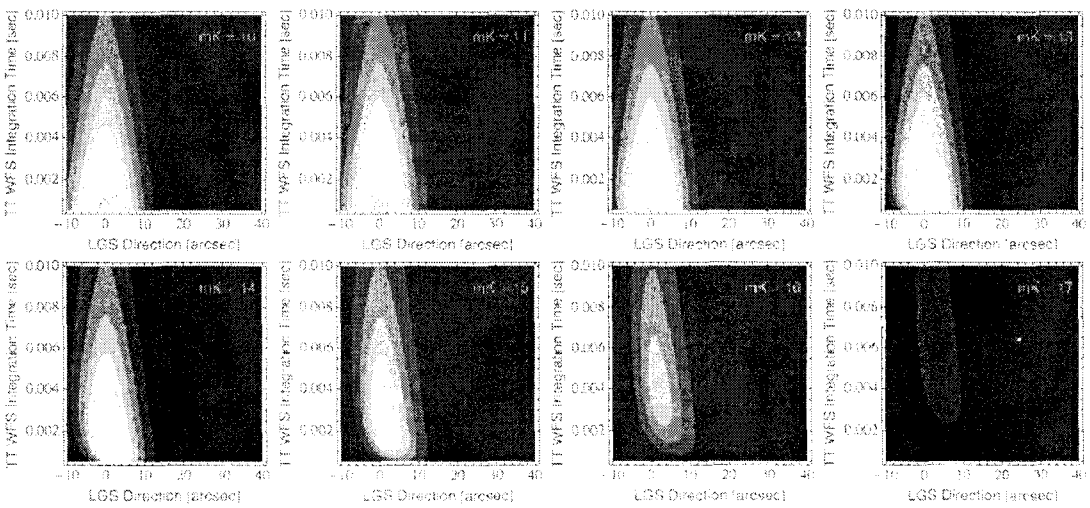

Figure 5. Science target H-band EE performance contours for tip-tilt NGS located 30" from the science target, having magnitudes between $10 < m_K < 17$. Each frame plots Strehl ratio in 2.5% contours for a range of tip-tilt sensor integration times, T_{TInt}, and LGS pointing, θ_{LGS}.

ACKNOWLEDGMENTS

This work has been supported by the National Science Foundation through grant AST-0619922.

REFERENCES

1. R. G. Dekany, C. Neyman, and R. Flicker, "Sharpening of natural guide stars for low-order wavefront sensing using patrolling laser guide stars," *Proc. SPIE* **7015**, pp. 701525–701525–10, 2008.
2. R. G. Dekany, B. Bauman, D. Gavel, M. Troy, B. Macintosh, and M. Britton, "Initial concepts for CELT adaptive optics," *Proc. SPIE* **4839**, pp. 1165–1174, 2003.
3. P. L. Wizinowich, D. L. Mignant, A. H. Bouchez, R. D. Campbell, J. C. Y. Chin, A. R. Contos, M. A. van Dam, S. K. Hartman, E. M. Johansson, R. E. Lafon, H. Lewis, P. J. Stomski, D. M. Summers, C. G. Brown, P. M. Danforth, C. E. Max, and D. M. Pennington, "The W. M. Keck Observatory laser guide star adaptive optics system: Overview," *Publications of the Astronomical Society of the Pacific* **118**, pp. 297–309, 2006.
4. P. Y. Bely, *The Design and Construction of Large Optical Telescopes*, Springer, New York, N.Y., 2006.
5. A. Marechal *Rev d'Optique* **26**, p. 257, 1947.
6. R. J. Sasiela and J. D. Shelton, "Transverse spectral filtering and mellin transform techniques applied to the effect of outer scale on tilt and tilt anisoplanatism," *JOSA A* **10**, pp. 646–660, 1993.
7. J. W. Hardy, *Adaptive Optics for Astronomical Telescopes*, Oxford University Press, New York, N.Y., 1998.
8. D. G. Sandler, S. Stahl, J. R. P. Angel, M. Lloyd-Hart, and D. McCarthy, "Adaptive optics for diffraction-limited infrared imaging with 8-m telescopes," *JOSA A* **11**, pp. 925–945, 1994.